Midfidelity model verification for a point-absorbing wave energy converter with linear power take-off

Eirini Katsidoniotaki, Yi-Hsiang Yu, Malin Göteman

Abstract—**In the preliminary design stage of a wave energy converter (WEC), researchers need fast and reliable simulation tools. High-fidelity numerical models are usually employed to study the wave-structure interaction, but the computational cost is demanding. As an alternative, midfidelity models can provide simulations in the order of real time. In this study, we operate Uppsala University's WEC in a relatively mild sea state and model it using WEC-Sim. The model is verified based on OpenFOAM simulations. To analyze the ability of the midfidelity model to capture WEC dynamics, we investigate the system separately with 1, 2, and 3 degrees of freedom. We examine the contribution of viscous phenomena, and study both linear and weakly nonlinear solutions provided by WEC-Sim. Our results indicate that the viscous effects can be neglected in heave and surge motion, but not for pitch. We also find that the weakly nonlinear WEC-Sim solution successfully agrees with the computational fluid dynamics, whereas the linear solution could suggest misleading results.**

Index Terms—**CFD, hydrodynamic analysis, numerical simulations, offshore renewables, point-absorber, verification, wave energy, wave-structure interaction, WEC-Sim.**

I. Introduction

THE amount of energy enclosed in ocean waves has been classified as one of the most promising renewable energy sources [1], [2]. Although attempts to utilize this resource date back to at least 1890, wave power is currently not widely employed. Nowadays, different wave energy conversion systems are being investigated, but only a few concepts have been operated in a sea environment. According to the Joint Research Centre Ocean Energy Database, only a few devices have reached technology readiness level (TRL) 8. The TRL ranges between 5 and 8 for most of the devices, which means their commercial readiness is yet to be proven [3].

High-fidelity computational fluid dynamics (CFD) simulations can resolve nonlinear hydrodynamic effects associated with wave-structure interaction, but the computational time for some applications is prohibitive. In a workshop on WEC extreme conditions modeling [4] hosted by Sandia National Laboratories and the National Renewable Energy Laboratory, the improvement of numerical modeling was discussed, and one of the recommendations involves using lower-fidelity models in the initial stage of the WEC design process (Appendix C.1.2.2). The lower-fidelity models can be employed to analyze the response of the device in several conditions for a given deployment location, and propose critical evaluation points in which high-fidelity models subsequently are employed.

Midfidelity numerical models, such as WEC-Sim, provide linear-time-domain solutions [5]. These codes apply radiation and diffraction methods to predict the response of the system. The hydrodynamic forces are calculated from the linear coefficients obtained by boundary-element-method codes, and the system dynamics are solved in the time domain. The simulation time is typically in the order of real time. Many studies for WEC devices have employed WEC-Sim, leading to successful results such as the development of a dual-flap floating oscillating surge WEC [6], an oscillating surge WEC [7], and the RM3 model based on a point-absorbing concept, which is one of the WEC reference models of the U.S. Department of Energy [8].

Nonlinear phenomena, including viscous damping and overtopping, have been identified as a source of uncertainty in lower-fidelity models [9]–[11]. In particular, the viscous damping effect is caused by flow separation and vortex shedding around the floating structure. In WEC-Sim, the viscous force is implemented via the Morison quadratic damping term, which depends on the drag coefficients and the characteristic area. The drag coefficient needs to be estimated prior to the calculations, and one can determine this coefficient from experimental or CFD results. In addition, a

Manuscript received 13 December, 2021; published 10 June, 2022. This article has been subject to single-blind peer review by a minimum of two reviewers. This work was supported by the Centre of Natural Hazards and Disaster Science (CNDS) in Sweden, the Swedish Research Council (VR, grant number 2015-04657), the Swedish Energy Authority (project number 47264-1). This scientific paper was also supported by the Onassis Foundation, scholarship ID: F ZP 021-1/2019-2020. This work was also authored by the National Renewable Energy Laboratory, operated by Alliance for Sustainable Energy, LLC,for the U.S. Department of Energy (DOE) under Contract No. DE-AC36-08GO28308.

Eirini Katsidoniotaki is PhD candidate at the Department of Electrical Engineering, Division of Electricity at Uppsala University. Lägerhyddsvägen 1, 752 37, Uppsala Sweden. (e-mail: eirini.katsidoniotaki@angstrom.uu.se).

Yi-Hsiang Yu is Senior Researcher in the Water Power Program at National Renewable Energy Laboratory. 15013 Denver W Pkwy, Golden, CO 80401, United States. (email: yi-hsiang.yu@nrel.gov)

Malin Göteman is Associate Professor at the Department of Electrical Engineering, Division of Electricity at Uppsala University. Lägerhyddsvägen 1, 752 37, Uppsala Sweden. (e-mail: malin.goteman@angstrom.uu.se).

Digital Object Identifier: https://doi.org/10.36688/imej.5.67-75

weakly nonlinear formulation is often used to account for the nonlinear buoyancy and Froude-Krylov forces, induced by the instantaneous free surface elevation and body position. As presented in [12], [13] WEC-Sim was applied in a study as part of the Collaborative Computational Project in Wave Structure Interaction 2 (CCP-WSI) Blind Test Series 2 for a hemispherical-bottomed cylinder and a truncated cylinder with a cylindrical moon pool under series of focused waves.

In [14], the experimental data from physical wave tank tests were used for the estimation of the viscous drag coefficients for the Uppsala University WEC modeled in WEC-Sim. In particular, the viscous drag coefficient for the heave motion was estimated via free decay experimental tests, and for the surge motion the coefficient was obtained through regular wave experiments. It was concluded that the heave viscous drag coefficient is well-tuned, but it is not suggested as an accurate value for the surge viscous drag coefficient. Moreover, it is worth mentioning that the experimental tests did not include a power take-off (PTO) system, leading to two main disadvantages: first, the WEC-Sim model does not represent the model in the real operational mode, and second, the relative velocity of the system (which is related to viscous effects) is dependent on the presence of PTO.

In this study, a WEC-Sim model of the Uppsala University WEC is developed and verified with OpenFOAM results. The WEC consists of a direct-driven linear PTO system and operates in a relatively mild sea state, so as to avoid the highly nonlinear phenomena occurring in more energetic sea states [15]. WEC-Sim solves the complex hydrodynamics associated with wave-structure interaction and electro-mechanical dynamics from the power take-off; therefore, it is highly important to use the correct definition of the restraints acting on the system. For better understanding of the WEC's response, the numerical model is constrained to move in 1 degree of freedom (DoF), 2 DoF, and 3 DoF, and each case is investigated separately. As suggested by [8], the weakly nonlinear restoring and Froude-Krylov forces may need to be included in the preliminary design-load evaluation stage with the use of a midfidelity model. In the framework of the present work, the nonlinear and linear solutions offered by WEC-Sim are compared with the CFD results, and prove that the linear approach could produce misleading conclusions. Furthermore, for the proper calibration of the WEC-Sim model, the viscous drag coefficients need to be adjusted. Following the recommendation from [4] regarding the potential improvement of numerical modeling, the viscous parameters can be predicted via CFD for use in lower-fidelity models. As a contrast to the work in [14], the current method uses a linear PTO system and the buoy has different configuration, implying that the viscous drag coefficients cannot be retrieved from the results in [14]. The long-term goal of this study is to develop a reliable WEC-Sim model of the Uppsala University WEC and utilize it for future investigation in extreme sea states.

II. Uppsala University's wave energy conversion system

Uppsala University's WEC has a vertical cylindrical buoy that is 3.4-m in diameter and 2.12-m in height. The mass of the buoy is 5,736 kg, and the center of gravity is 0.24 m below the still water level. The translator of the PTO system pulls the buoy down due to the translator weight, and the buoy has an initial draft of 1.3 m. The mass of the translator is 6,240 kg. The buoy is connected to the PTO through a connection line. Fig. 1 shows the PTO system of Uppsala University's WEC, which is a direct-driven linear generator that has only vertical internal movement.

The forces on the buoy consist of the hydrodynamic forces due to wave-structure interaction, the weight of the buoy, and the force in the connection line. Due to the connection line, the motion of the buoy and the translator is coupled, and the forces from the PTO are transferred to the buoy. These forces are the translator weight, the generator damping, force from the upper end-stop spring, and friction due to the translator motion. When the translator exceeds the free stroke length of 1.2 m and hits the upper end-stop spring of the PTO, a force from the spring, F_{spring}, acts downward. When the upper spring is fully compressed, the connection wire acts as an elastic mooring cable, which adds further restraint force, F_{add}, in the system. The spring stiffness is 776 kN/m and has a compression length of 0.6 m, whereas the connection line stiffness is 300 kN/m. The electromagnetic damping force in the generator, F_{PTO}, is proportional to the translator velocity and acts in the opposite direction of the translator motion. The damping coefficient is 5 kNs/m. When the translator exceeds the lower free-stroke length, it rests at the lower position of the generator hull, then the connection line slacks and the motion of the buoy becomes uncoupled.

When the line is not slack, the motion of the buoy and the translator is coupled through the connection line. The restraints from the PTO acting on the buoy are expressed via the restraint force, F_{line}, which is directed along a vector from the center of the buoy's bottom surface to a fixed anchor point, as seen in Fig. 2. The total force acting on the buoy is the sum of the hydrodynamic forces, the restraint force, and the weight of the buoy.

In OpenFOAM, the above-described motion is applied by an in-house developed restraint described by the following equations:

$$m_b\ddot{r}(t) = \iint p\hat{n}dS + F_{\text{line}} - m_b\overline{g} \tag{1}$$

$$F_{line} = \delta_{down}(-m_t g + F_{\text{PTO}} - F_{\text{spring}} - F_{\text{add}})\hat{r} \tag{2}$$

where m_b and m_t is the mass of the buoy and translator, respectively, and r is the position vector of the buoy. The damping force from the generator is $F_{PTO} = -\gamma\dot{r}(t)$, with γ being the damping coefficient in Ns/m. The spring force F_{spring} and the additional elastic mooring force F_{add} are nonzero only when the

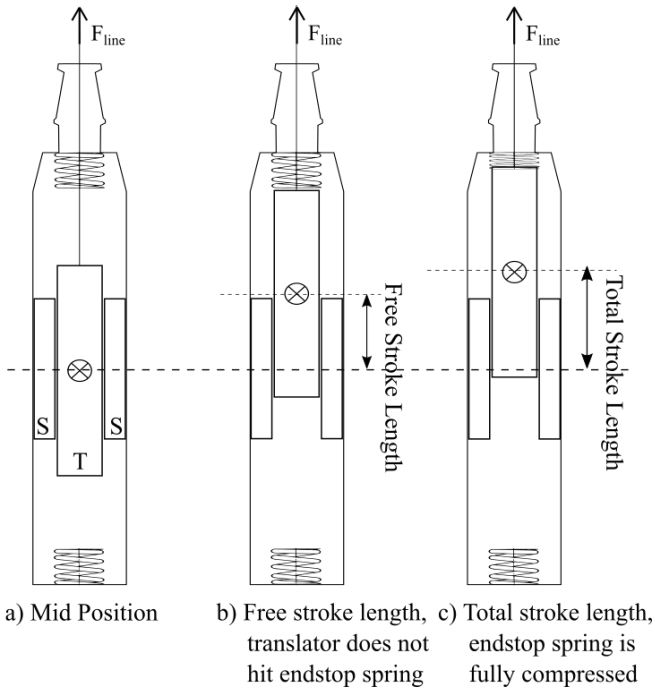

Fig. 1. The direct driven linear generator of Uppsala University's WEC [16]. The generator is placed on the seabed and directly driven by the floating body through the connection wire.

translator position exceeds the free and total stroke lengths, respectively:

$$F_{spring} = \begin{cases} k_{spring}(r - r_{rest}) & \text{if } (r - r_{rest}) > 1.2 \\ 0 & \text{otherwise} \end{cases} \quad (3)$$

$$F_{add} = \begin{cases} k_{mooring}(r - r_{rest}) & \text{if } (r - r_{rest}) > 1.8 \\ 0 & \text{otherwise} \end{cases} \quad (4)$$

When the translator exceeds the downward stroke length, the line slacks. This is implemented through the δ_{down}:

$$\delta_{down} = \begin{cases} 1 & \text{if } (r - r_{rest}) > -1.2 \\ 0 & \text{otherwise} \end{cases} \quad (5)$$

where k_{spring} and $k_{mooring}$ is the spring and mooring line stiffness, respectively, r_{rest} is the line length when the buoy is resting when the water level is still, the length of the upward/downward free-stroke length is equal to 1.2 m, and the total stroke length is equal to 1.8, as seen in Fig. 1.

III. Sea state

The Uppsala University WEC is simulated in a relatively mild sea state, so as to avoid highly nonlinear effects connected to extreme wave events. The wave height, H, is 4 m and the wave period, T, is 8 s at a sea location with water depth of 40 m. According to [17], the wave is considered a Stokes 2nd-order regular wave with approximately 4% steepness.

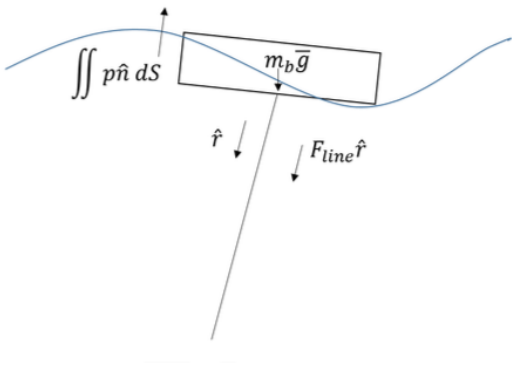

Fig. 2. The forces acting on the buoy are the sum of hydrodynamic and gravitational forces, as well as the forces from the generator. The F_{line} is directed toward an anchor point [16].

IV. Numerical models

A. WEC-Sim model

WEC-Sim is the midfidelity numerical model utilized in this study for solving the wave-structure interaction dynamics in time domain, based on the radiation and diffraction method. A detailed description of the theory, methodology, validations, and applications of WEC-Sim toolbox are provided in [5], [18], [19].

The dynamic response of the system is calculated by solving the WEC system equation of motion (Cummins equation) around the center of gravity of the buoy, given as:

$$(m + m_\infty)\ddot{x} = -\int_{-\infty}^{t} K(t-\tau)\dot{x}(\tau)d\tau - F_{hs} + F_e + F_\nu + F_{ext} \quad (6)$$

where m and m_∞ are the mass matrix and added mass matrix at the infinite frequency, respectively. x is the position vector, the term $-\int_{-\infty}^{t} K(t-\tau)\dot{x}(\tau)d\tau$ is the convolution integral representing the resistive force on the buoy due to the wave radiation, K is the impulse response function, and F_{hs}, F_e, F_ν, and F_{ext} are the hydrostatic restoring force, the wave excitation force, the viscous drag force, and the external force, respectively. The linear force coefficients m_∞, K, F_{hs}, F_e usually are obtained from boundary-element-method simulations. For that purpose, WAMIT code [20] was applied here.

In our study, a weakly nonlinear approach is applied, considering nonlinear hydrodynamic forces induced by the instantaneous water surface elevation and body position. In this latter case, instead of using the boundary-element-method-calculated linear wave-excitation and hydrostatic coefficients, the nonlinear buoyancy and Froude-Krylov forces are obtained by integrating the static and dynamic pressures along the wetted body surface at each time step. The geometry STL file is notably important because it is used as the discretized body surface on which the nonlinear pressure forces are integrated. For that reason, a good mesh resolution is required [5]. The mesh refinement, as shown in Fig. 3, was performed using the CAD software Rhino [21].

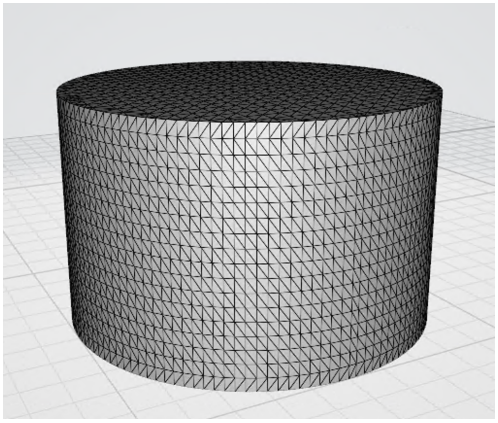

Fig. 3. Discretized surface for the cylindrical buoy with approximately 4,000 panels, used for nonlinear buoyancy and Froude-Krylov pressure calculations in WEC-Sim.

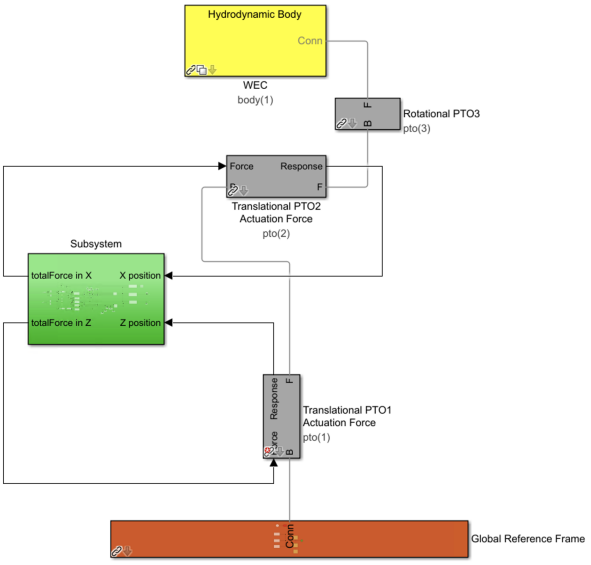

Fig. 4. WEC-Sim Simulink model of the Uppsala University WEC.

1) Set-up: The WEC-Sim model consists of the Simulink model, shown in Fig. 4, and the MATLAB input file, in which the simulation parameters (e.g., wave properties, hydrodynamic coefficients, buoy properties, viscous drag coefficients, PTO characteristics) are all specified. The Simulink model was created using prebuilt WEC-Sim blocks. In particular, three PTO blocks were utilized for the 3 DoF motion, two of them control the translational motion (heave and surge), and the third the rotational motion (pitch). Each one of the translational PTO uses an actuation force, which is defined in the block "subsystem" and depends on the system's position and velocity at every time step.

For the regular wave simulations, a ramp time of 2 T is used, and the simulation time is 15 T, which is the same for the CFD simulations and allows a direct comparison, with variable time step. The WEC-Sim models were run on a desktop computer with twelve 3.70-GHz processors. The simulation time for the case with 3 DoF and linear solution was approximately 2 min, meaning that the simulation time is almost the same as real time. However, the simulation time for the weakly nonlinear solution was approximately 4 min.

2) Viscous drag coefficients: In WEC-Sim, the viscous damping is included via additional Morison-like quadratic damping term. The Morison equation provides a semi-empirical formulation to model the unsteady force on rigid structures in oscillatory flow [22]. For a 3D structure moving in-line with the oscillatory flow, the Morison equation is:

$$F(t) = \rho V C_m(\ddot{X} - \dot{U}) + \frac{1}{2}\rho A_r C_d(U - \dot{X})\left|U - \dot{X}\right| \quad (7)$$

where t is the time, ρ is the fluid density, V is the volume of the structure, C_m is the inertial coefficient, X is the body position, U is the fluid velocity, A_r is the relevant cross-sectional area, and C_d is the drag coefficient. In the right-handed part of Morison equation, the first term expresses the inertia force, and the second term the drag force.

The intensity of the viscous damping term depends on the coefficient in each DoF, which needs to be estimated prior to the calculations. The estimation cannot be considered a trivial process. These coefficients can be obtained from experimental measurements, numerical simulations, or previously reported values [23]–[26]. The viscous force is the result of the skin friction effect, flow separation, and eddies contribution. In this study, the coefficients are estimated through CFD simulations. In particular, the CFD force time series is fitted in the Morison equation using a least-square approach. The term of the Morison viscous force is proportional to the cross-sectional area of the moving structure. This area for heave mode is $9m^2$, for surge mode is $4.42m^2$, and for pitch mode is $2.43m^5$.

There is a useful degree of correlation between the coefficients and two flow parameters—the Keulegan–Carpenter number, KC, and the Reynolds number, Re—defined as:

$$KC = 2\pi\alpha/D \quad (8)$$

$$Re = U_m D/\nu \quad (9)$$

where α is the amplitude of the structure displacement, D is the diameter of the buoy, T is the wave period, U_m is the maximum amplitude of the sinusoidal velocity, and ν is the kinematic viscosity of the fluid. For large Reynolds numbers, the inertial force dominates and the viscous effects degrade. In this study, $Re = 5.3 \cdot 10^6$, and $KC = 3.7$. The KC is rather low and the Reynolds number large, suggesting that the viscous forces are small compared to the inertial forces, which is confirmed by the CFD solution. Here, the viscous drag coefficients for heave and surge mode are calculated to be less than 0.05, so they can be neglected. Even though the pitch moment due to the pressure forces is significantly higher than the viscous forces, the latter can not be excluded because the pitch viscous coefficient is estimated equal to 8. From CFD simulations, it can be concluded that for the case with 3 DoF, the viscous effects for heave and surge motions are slightly more significant compared to cases with 1 DoF and 2 DoF, but still can be neglected.

B. CFD model

OpenFOAM-v1906 is utilized in this study for the high-fidelity CFD simulations. The two-phase incompressible unsteady Reynolds averaged Navier-Stokes (RANS) equations solver interFoam is used for tracking the free surface, including mesh motion and deformation capability. The solver is based on the volume of fluid method, and the interface is indirectly represented by a numerical field describing the volume fraction of water within each computational cell. The physical properties are calculated as weighted averages based on this function. The solver uses the PIMPLE algorithm for pressure-velocity coupling.

The motion of the buoy is calculated through the `sixDoFRigidBodyMotion` library, based on Newton's law. The forces acting on the buoy are the sum of the hydrodynamic forces and any additional user-defined forces. In the present application, the connection of the buoy with the PTO system is described by an in-house developed restraint, as described in Section II. The buoy is also constrained to move only in the designated DoF, and within the framework of the present work the buoy can move only in (i) heave, (ii) heave-surge, and (iii) heave-surge-pitch DoF. The morphing dynamic mesh method is applied to capture the mesh morphing change over time due to the prescribed motion, because the sea state does not lead to high mesh deformations.

The computational domain length is adjusted 2λ in front, and 4λ behind the buoy. The depth is 40 m, and the width is 1λ. Specific boundary conditions included in the IHFOAM toolbox allow the generation and absorption of any type of wave in the 3D domain applying the static boundary method. One of the favorable characteristics of IHFOAM is the reduced computational cost [27] and has been recently launched by OpenFOAM, supporting the simulation of offshore engineering processes [28]. Similar studies have utilized the same toolbox [29]–[31].

The computational grid is generated and refined using the snappyHexMesh library in such a way that the mesh is refined in the vicinity of the water surface and buoy, reducing the computational cost. The resulting grid resolution in the refinement region around the water surface is $H/\Delta z = 10$ in the vertical direction and $\lambda/\Delta x = 250$ in the horizontal direction, keeping the aspect ratio equal to 1. The mesh resolution for the current application is based on the recommendations provided by [32] when mild sea states are examined. Moreover, two even finer regions are added around the buoy, and the boundary layer is generated in order to ensure a value of $y+ \in [30, 200]$ [33]. In Fig. 5, the refinement regions around the buoy and water surface are shown, but the boundary layer cannot be depicted due to the small size of the cells. In an attempt to reduce the computational grid size, the mesh grading technique is applied in x, y, and z directions far from the buoy. The total mesh size is 3.3×10^{-6}.

The NWT consists of six patches, each assigned with appropriate boundary conditions for every variable. The wave velocity is defined at the inlet, and the pressure at the outlet. The bottom and side patches are defined as slip walls. The initial values of the turbulence model SST $k-\omega$ are related to the celerity of the incoming wave, with k being the turbulence kinetic energy, while ω is the specific rate of dissipation. In this study, wall functions are employed to approximate the turbulence in the near-wall region, and the first cell is centered in the log-law region, ensuring the accuracy of the result.

A variable time step is defined as ensuring numerical stability and accuracy through a Courant number of 0.5, using first-order implicit solver. Each simulation is run for $15T$ on a high-performance computer cluster. On average, each simulation required 13 hr using 128 CPU, for a total of approximately 1,664 CPU·hr.

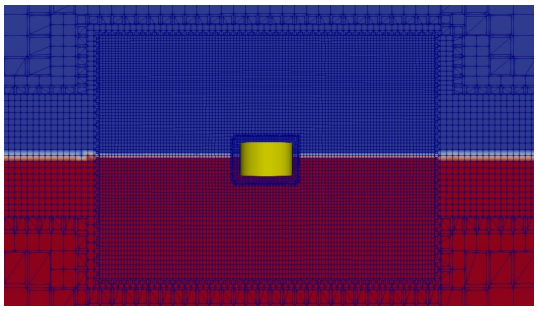

Fig. 5. The mesh is refined in the vicinity of the buoy. There is an outer refinement box surrounding the buoy and even finer region closer to the buoy, which contains the boundary layer. For adequately capturing the wave propagation, the refined region is applied in the water surface.

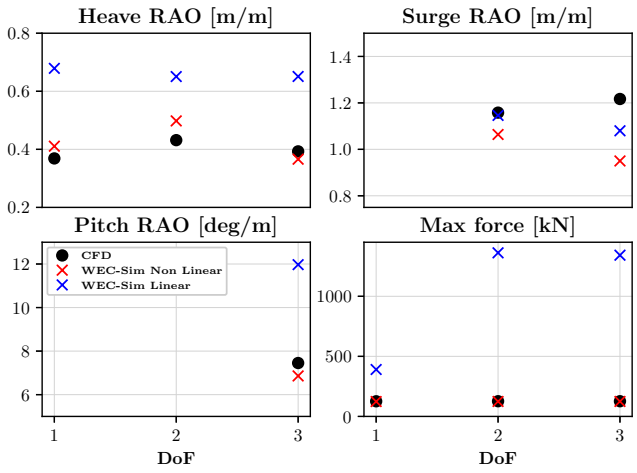

Fig. 6. The RAOs for heave, surge, and pitch motion for cases with 1, 2, and 3 DoF, as calculated by mid and high-fidelity solvers. The maximum force in the connection line is also depicted in the lower-right plot. In terms of the midfidelity model, the linear and weakly nonlinear approaches are also compared.

V. Results

A. Mid and high-fidelity numerical models

The Uppsala University WEC was examined for 1 DoF, 2 DoF, and 3 DoF using mid and high-fidelity numerical simulations. The heave, surge, and pitch RAOs, as well the maximum force in the connection line, are summarized in Fig. 6 for all the examined cases.

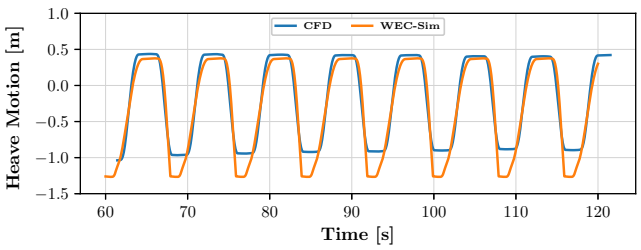

Fig. 7. Heave response time series for WEC moving only in heave (1 DoF case)

First, this study investigates the WEC's response subjected only to heave motion (1 DoF case). Fig. 7 shows the time series as solved using mid and high-fidelity models. The two solutions agree well, especially when the buoy follows the wave crest motion, whereas during wave troughs the WEC-Sim model is subjected to deeper displacements. According to Uppsala WEC restraint (see Section II), the force from the PTO acts as an external force on the buoy; however, when the PTO force gains upward direction (i.e., downward buoy motion), the external force is set to zero. During the simulations, the external PTO force stops acting 2 s after the buoy is moving from the highest to the lowest position, meaning the motion of the buoy is controlled only through the hydrodynamic forces, its own weight, and buoyancy force. The deviation in trough displacements, shown in Fig. 7, accounts for the undisturbed regular wave profile generated in WEC-Sim, whereas in CFD the observed surface elevation process is positively skewed with higher crests and shallower troughs. Overall, considering only 1 DoF buoy motion, WEC-Sim provides the solution for the heave displacement with 11% divergence from the solution, as calculated by OpenFOAM. The force in the connection line is mainly dependent on the upward buoy motion, justifying the fact that the maximum line forces are almost identical for both solutions.

At the second stage of this study, the WEC is allowed to move in heave and surge DoF (2 DoF case), and the responses are presented in Fig. 8. Comparing the heave RAOs, the deviation of the results between the two solutions is slightly higher, around 15%, showing that the heave motion is affected by the introduction of the surge DoF. In addition, noticing the heave time series as given by CFD, an oscillation on the upper plateaus is recorded, which is not captured by the midfidelity model. As seen in Fig. 9a and b, the wave overtopping is slightly more pronounced, introducing further nonlinearities into the solution once surge DoF is added. However, it is worth mentioning that by allowing the WEC to move also in surge, the range of heave displacement is increased both for mid and high-fidelity solutions. In terms of the surge motion, the time series—as calculated by the two fidelity models—follow a similar pattern, expressed as 9% deviation in surge-RAOs. The maximum force in the connection line still has almost identical values for the two solutions.

Finally, the Uppsala University WEC model was subjected to 3 DoF motion: heave, surge, and pitch.

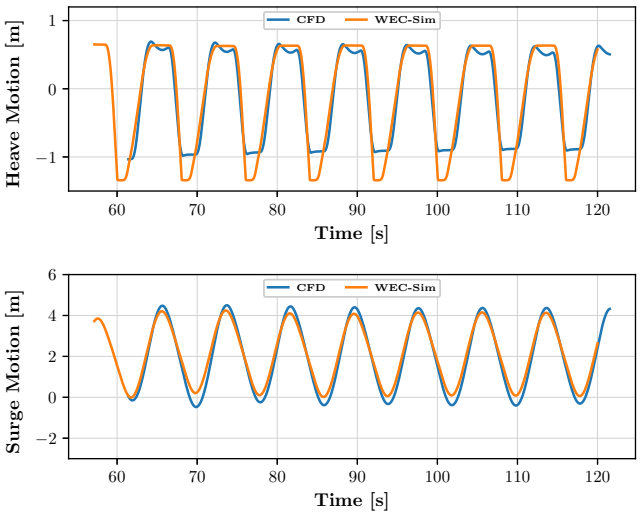

Fig. 8. The WEC is restricted to move only in heave and surge direction (2 DoF case). The upper plot represents the time series of heave motion, and the lower plot shows the surge motion.

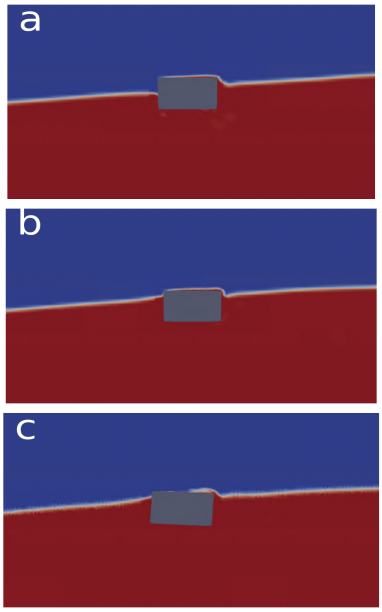

Fig. 9. Wave overtopping for the WEC moving (a) only in heave, (b) in heave and surge DoF, (c) in heave, surge, and pitch DoF. The phenomenon is more intense for the case with 2 DoF motion, but the introduction of the pitch motion slightly eliminates the wave overtopping.

Looking at Fig. 9c, one could say that the pitch motion slightly alleviates the WEC from wave overtopping effect. Fig. 10 presents the WEC's response in 3 DoF motion. Introducing the pitch motion, the deep through displacements as observed in the previous two WEC-Sim solutions stop occurring. Instead, the heave response comes in better agreement with the CFD solution. On the other hand, the surge response for the case with 3 DoF appears to have greater deviation compared to the case with 2 DoF. It seems that the surge motion is smaller when the pitch motion is added, according to WEC-Sim solution. Fig. 11 depicts the time series of the force in the connection line. As has been already mentioned, the force is highly dependent on

the heave motion during the wave crests, therefore, the force is again well-predicted by WEC-Sim. The response of pitch motion changes depending on the implemented fidelity model. Further investigation was conducted to explain the fact that the pitch motion is not well-captured by WEC-Sim. Two more waves were investigated, keeping the same wave height but changing the wave period. Note that the wave examined in the present work has the following characteristics: H = 4 m, T = 8 s, and $steepness$ = 4%. The shorter wave has period 6 s, and the longer wave has period 10 s, with steepness 7% and 2.7%, respectively. As can be seen in Fig. 12, the buoy has limited range of pitch motion for wave steepness 2.7%, thus, the pitch RAOs for the two fidelity solutions come in better agreement. For the case of wave steepness 7%, the range of pitch motion is more pronounced, leading to higher deviation between the solutions.

Similar observation has been also reported in [13], where the results obtained from the WEC-Sim has a better agreement with the CFD solutions and the experimental values for the heave and surge motions, including the prediction of the drift, when the weakly nonlinear formulation was applied. However, the differences between the WEC-Sim solution and CFD simulated or measured pitch responses were relatively higher. The difference in pitch that was shown in this study and in [13] could be attributed to the selection of viscous drag coefficients, and the limitation of weakly nonlinear model. In particular, when using the weakly nonlinear formulation, the buoyancy and Froude-Krylov forces are calculated based on the instantaneous free surface elevation and body position. However, the radiation and wave scattering coefficients are still calculated based on linear theory in the WEC-Sim simulations. Further investigation will be needed in future studies.

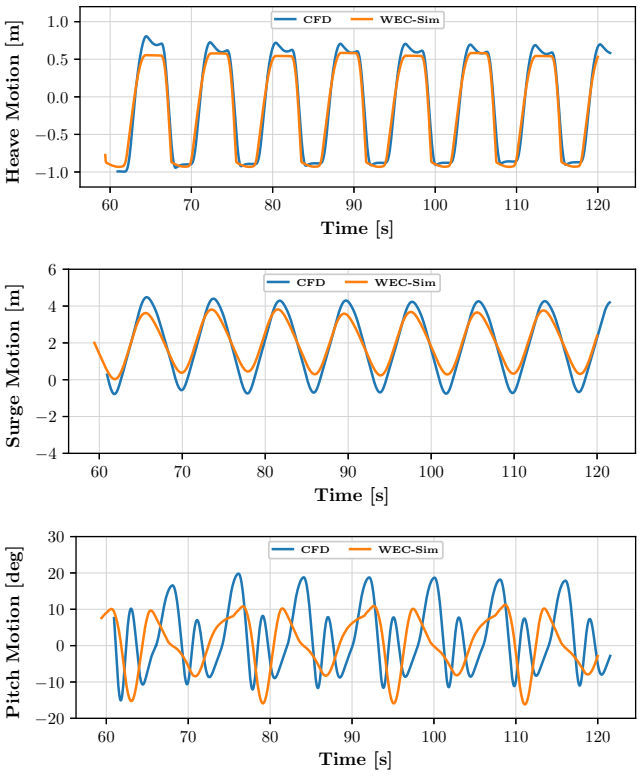

Fig. 10. The WEC is restricted in heave, surge, and pitch motion (3 DoF case). The upper plot represents the time series of heave response, the middle plot the surge response, and the lower plot the pitch response.

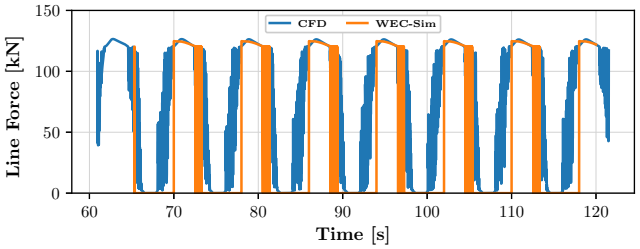

Fig. 11. The WEC is restricted in 3 DoF motion. The plot represents the time series of the connection line force.

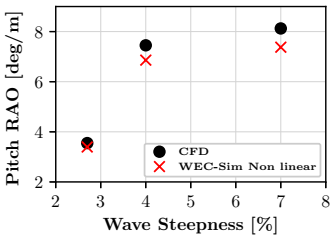

Fig. 12. The pitch-RAOs for high- and midfidelity are compared in conjunction with the wave steepness. For a wave with lower steepness, the buoy pitch motion becomes more pronounced, and the deviation between the two solutions is larger.

B. Linear and nonlinear solution

The midfidelity model is solved using two different approaches; the first uses a fully linear hydrodynamic model, and the second uses nonlinear hydrostatic and Froude-Krylov forces, calculated from the instantaneous position of the buoy. The results are compared in Fig. 13, with the CFD solution as a reference. Moreover, in Fig. 6, the RAOs for heave, surge, pitch motion, and the maximum line force are compared for the linear solution (blue cross), the nonlinear solution (red cross), and CFD (black circle).

The heave response is highly dependent on the selected approach; the nonlinear solution comes in better agreement with the CFD solution, whereas the linear solution significantly deviates, having a larger range of motion. In the Uppsala University WEC, the force in the connection line is mainly driven by the heave buoy motion and expresses the external forces acting on the buoy due to the presence of the PTO. For the linear solution, the translator hits the upper end-stop spring, located on the top of the generator hull, creating snap loads of approximately 1,300 kN. These snap loads correspond to the extra force due to the compression of the upper-end stop spring and the stiffness of the mooring line, which reacts like a spring. On the other hand, according to the CFD and nonlinear midfidelity model, the upper end-stop spring is never compressed and the maximum force is equal to 125 kN. This force expresses the sum of the PTO damping force, friction force, and translator weight.

As far as the surge response is concerned, the surge RAO calculated applying the linear approach comes in better agreement to the CFD solution; yet, in the time series plots, the linear WEC-Sim solutions present an offset. This leads to the conclusion that the offset is related to the higher-order drift forces, which are not well-captured by a midfidelity model.

Last but not least, the pitch motion also differs considerably for the linear and nonlinear solutions, highlighting the significant effects of nonlinear phenomena. According to the linear approach, the pitch is expressed by a sinusoidal motion with great range of oscillation. In fact, for the present application, the simulation of pitch motion seems to be a nontrivial task for the WEC-Sim model, and neither of the two approaches matches well with the CFD solution.

In general, the nonlinear midfidelity solution is closer to the high-fidelity solution because the hydrostatic and Froude-Krylov forces are calculated by integrating over the buoy's instantaneous wetted surface, with respect to the free water surface. Therefore, the nonlinear solution leads to more accurate results. Fig. 14 depicts the sum of buoyancy and Froude-Krylov forces acting in the z-direction, as calculated by WEC-Sim. The significant change in the instantaneous buoy position is the reason for the sharp changes of the nonlinear solution. The total force acting on the buoy, in an upward direction, is higher for the linear solution, justifying the greater heave displacement.

VI. Discussion

In this study, the Uppsala University WEC is evaluated and compared using RANS CFD simulations (OpenFOAM) and a potential flow-based model, WEC-Sim. For the verification study, the WEC is investigated in a relatively mild sea state, so as to avoid high nonlinear phenomena present in extreme wave conditions. The main focus of this work is the development of a realistic WEC-Sim model with a PTO restraint matching accurately to the equivalent restraint applied in OpenFOAM, and expressing the Uppsala University WEC in normal operational conditions. To analyze the WEC's response, the system is evaluated separately in 1 DoF, 2 DoF, and 3 DoF. The quantities of interest are the RAO in heave, surge, and pitch motion, as well as the maximum force in the connection line, which is a critical mechanical subsystem.

The effect of viscous forces on the WEC are investigated, and the viscous damping coefficients are identified via the correlation of the Morisson equation with the forces as calculated by OpenFOAM. It can be concluded that the viscous forces affect the heave and surge motion of the buoy only to a minor extent, and can therefore be neglected. This conclusion comes into agreement with the high Reynolds number, which indicates that the inertia forces dominate over the viscous. However, we noticed that the pitch motion is more affected by the viscous phenomena; therefore, the viscous forces can not be neglected in the pitch DoF.

The comparison between the weakly nonlinear WEC-Sim and CFD model reveals that the heave RAOs

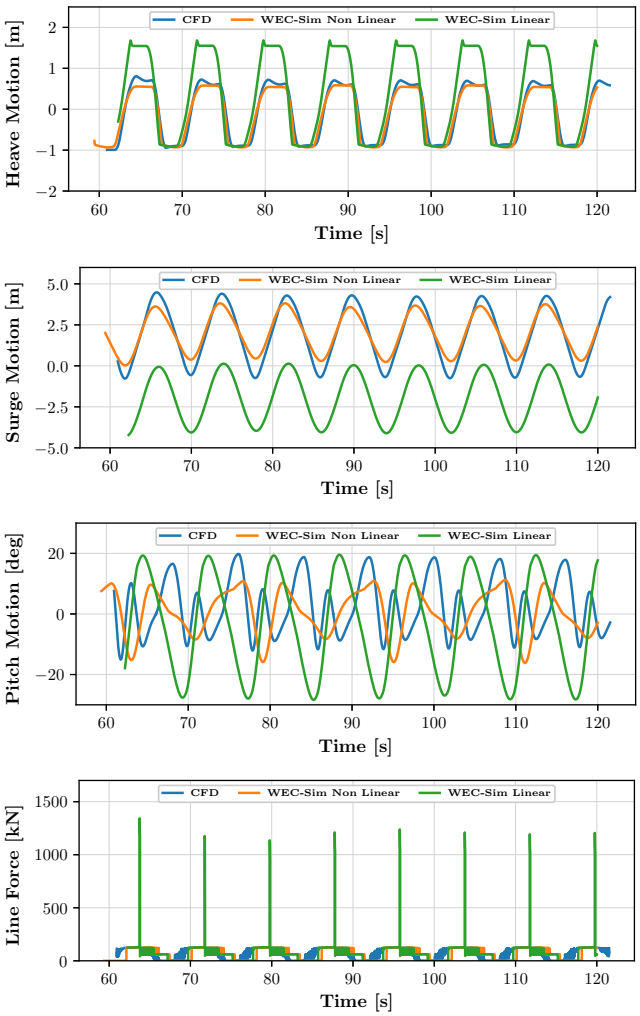

Fig. 13. The WEC is allowed to move in 3 DoF. The WEC-Sim model utilizes the linear and the weakly nonlinear approach for the calculation of the hydrostatic restoring and Froude-Krylov forces. The results are compared with the CFD solution, showing the importance of including the nonlinear effects.

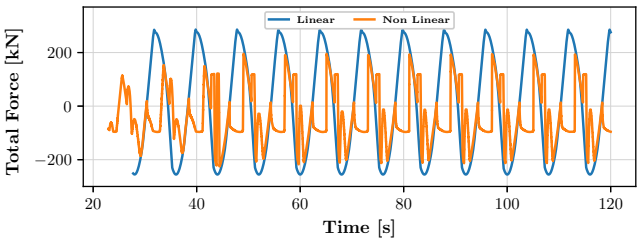

Fig. 14. Total force expresses the sum of the Buoyancy and Froude-Krylov forces in the z-direction, given by the WEC-Sim model using the linear and nonlinear solutions.

satisfactory agree when the WEC is allowed to move in 3 DoF, but this is not the case for the linear WEC-Sim solution. When the buoy is restricted in 1 DoF and 2 DoF motion, WEC-Sim indicates deeper through displacements during the heave motion. This disagreement is mainly due to the wave propagation profile; in WEC-Sim the wave profile is undisturbed, while in CFD the wave troughs are shallower. Moreover, the surge RAOs come in fair agreement for the two fidelity models. On the other hand, it seems to be a challenge for WEC-Sim to consider the pitch motion

in the present application. The simulation of pitch motion in WEC-Sim is sensitive to the wave steepness, because as long as the pitch motion is getting larger for steeper waves, it is more difficult to be caprtured by lower fidelity models. Last but not least, the maximum force in the connection line is well-estimated when the weakly nonlinear WEC-Sim is utilized, and the significant reduced computational time are encouraging evidences for its usage in the preliminary stage of the design process.

The comparison of two different solutions provided by WEC-Sim—the linear and nonlinear—specifies the importance of including the nonlinear phenomena. The linear solution tends to overpredict the results, which would lead to WEC's overdesign. Moreover, the linear solution shows the surge motion with an offset compared to the CFD results, and this is related to higher-order drift forces, which are not included in a midfidelity model.

For future studies, the WEC-Sim model could be investigated in extreme sea states and validated based on experimental extreme wave tank tests. Moreover, the WEC needs to be examined in 6 DoF motion. Furthermore, the adjustment of the viscous drag coefficients could be estimated based on experimental free decay tests and experimental wave-structure interaction tests. The pitch motion could be further investigated for a nonfixed center of rotation applications (e.g., point-absorbing WEC systems), and for determining how the effect of wave steepness could be reduced.

REFERENCES

[1] G. Mork, S. Barstow, A. Kabuth, and M. T. Pontes, "Assessing the global wave energy potential," in *International Conference on Offshore Mechanics and Arctic Engineering*, vol. 49118, 2010, pp. 447–454.

[2] P. T. Jacobson, G. Hagerman, and G. Scott, "Mapping and assessment of the united states ocean wave energy resource," Electric Power Research Institute, Tech. Rep., 2011.

[3] D. Magagna, R. Monfardini, and A. Uihlein, "JRC ocean energy status report 2016 edition," *Publications Office of the European Union: Luxembourg*, 2016.

[4] R. G. Coe, V. S. Neary, M. Lawson, Y. Yu, and J. Weber, "Extreme conditions modeling workshop report," National Renewable Energy Lab.(NREL), Golden, CO (United States), Tech. Rep., 2014.

[5] "WEC-Sim". [Online]. Available: https://wec-sim.github.io/WEC-Sim/

[6] K. Ruehl, D. D. Forbush, Y.-H. Yu, and N. Tom, "Experimental and numerical comparisons of a dual-flap floating oscillating surge wave energy converter in regular waves," *Ocean Engineering*, vol. 196, p. 106575, 2020.

[7] Y.-H. Yu, Y. Li, K. Hallett, and C. Hotimsky, "Design and analysis for a floating oscillating surge wave energy converter," in *International Conference on Offshore Mechanics and Arctic Engineering*, vol. 45547. American Society of Mechanical Engineers, 2014, p. V09BT09A048.

[8] J. van Rij, Y.-H. Yu, Y. Guo, and R. G. Coe, "A wave energy converter design load case study," *Journal of Marine Science and Engineering*, vol. 7, no. 8, p. 250, 2019.

[9] M.Atcheson. (May 2018) "Outline load assessment numerical tool", RiaSor2 (Reliability in a sea of risk). [Online]. Available: http://riasor.com/wp-content/uploads/2018/07/201805-RiaSoR-2-Outline-Load-Assessment-Numerical-Tool-Specification.pdf

[10] A. Babarit, J. Hals, M. J. Muliawan, A. Kurniawan, T. Moan, and J. Krokstad, "Numerical benchmarking study of a selection of wave energy converters," *Renewable energy*, vol. 41, pp. 44–63, 2012.

[11] Y.-H. Yu and Y. Li, "Reynolds-averaged Navier–Stokes simulation of the heave performance of a two-body floating-point absorber wave energy system," *Computers & Fluids*, vol. 73, pp. 104–114, 2013.

[12] J. van Rij, Y.-H. Yu, and T. T. Tran, "Validation of simulated wave energy converter responses to focused waves," *Proceedings of the Institution of Civil Engineers - Engineering and Computational Mechanics*, 2021. [Online]. Available: https://doi.org/10.1680/jencm.19.00039

[13] E. J. Ransley *et al.*, "Focused wave interactions with floating structures : A blind comparative study," *Proceedings of the Institution of Civil Engineers - Engineering and Computational Mechanics*, 2021.

[14] T. Tosdevin, M. Giassi, S. Thomas, J. Engstrom, M. Hann, J. Isberg, M. Goteman, E. Ransley, P. Musliedlak, and D. Simmonds, "On the calibration of a WEC-Sim model for heaving point absorbers," 2020.

[15] J. van Rij, Y.-H. Yu, A. McCall, and R. G. Coe, "Extreme load computational fluid dynamics analysis and verification for a multibody wave energy converter," in *International Conference on Offshore Mechanics and Arctic Engineering*, vol. 58899. American Society of Mechanical Engineers, 2019, p. V010T09A042.

[16] L. Sjökvist and M. Göteman, "Peak forces on wave energy linear generators in tsunami and extreme waves," *Energies*, vol. 10, no. 9, p. 1323, 2017.

[17] B. Le Méhauté, *An introduction to hydrodynamics and water waves*. Springer Science & Business Media, 2013.

[18] K. Ruehl, C. Michelen, S. Kanner, M. Lawson, and Y.-H. Yu, "Preliminary verification and validation of wec-sim, an open-source wave energy converter design tool," in *International Conference on Offshore Mechanics and Arctic Engineering*, vol. 45547. American Society of Mechanical Engineers, 2014, p. V09BT09A040.

[19] M. Lawson, Y.-H. Yu, K. Ruehl, and C. Michelen, "Development and demonstration of the WEC-Sim wave energy converter simulation tool," 2014.

[20] "WAMIT". [Online]. Available: https://www.wamit.com/

[21] "Rhinoceros". [Online]. Available: https://www.rhino3d.com/

[22] M. A. Bhinder and J. Murphy, "Evaluation of the viscous drag for a domed cylindrical moored wave energy converter," *Journal of Marine Science and Engineering*, vol. 7, no. 4, p. 120, 2019.

[23] B. Guo, R. Patton, S. Jin, J. Gilbert, and D. Parsons, "Nonlinear modeling and verification of a heaving point absorber for wave energy conversion," *IEEE transactions on sustainable energy*, vol. 9, no. 1, pp. 453–461, 2017.

[24] S. Jin, R. J. Patton, and B. Guo, "Viscosity effect on a point absorber wave energy converter hydrodynamics validated by simulation and experiment," *Renewable energy*, vol. 129, pp. 500–512, 2018.

[25] J. Journée and W. Massie, "Offshore hydromechanics," 2001.

[26] M. Lawson, B. B. Garzon, F. Wendt, Y.-H. Yu, and C. Michelen, "COER hydrodynamic modeling competition: Modeling the dynamic response of a floating body using the WEC-Sim and FAST simulation tools," in *International Conference on Offshore Mechanics and Arctic Engineering*, vol. 56574. American Society of Mechanical Engineers, 2015, p. V009T09A005.

[27] C. Windt, J. Davidson, P. Schmitt, and J. V. Ringwood, "On the assessment of numerical wave makers in cfd simulations," *Journal of Marine Science and Engineering*, vol. 7, no. 2, p. 47, 2019.

[28] P. Higuera, J. L. Lara, and I. J. Losada, "Realistic wave generation and active wave absorption for Navier–Stokes models: Application to OpenFOAM®," *Coastal Engineering*, vol. 71, pp. 102–118, 2013.

[29] H. Chen, L. Qian, Z. Ma, W. Bai, Z. Lin *et al.*, "CCP-WSI blind test series 3: OpenFOAM simulation of focused wave interaction with a simplified wave energy converter," in *The 29th International Ocean and Polar Engineering Conference*. International Society of Offshore and Polar Engineers, 2019.

[30] H. Chen, L. Qian, Z. Ma, W. Bai, Y. Li, D. Causon, and C. Mingham, "Application of an overset mesh based numerical wave tank for modelling realistic free-surface hydrodynamic problems," *Ocean Engineering*, vol. 176, pp. 97–117, 2019.

[31] C. Windt, J. Davidson, D. D. Chandar, N. Faedo, and J. V. Ringwood, "Evaluation of the overset grid method for control studies of wave energy converters in openfoam numerical wave tanks," *Journal of Ocean Engineering and Marine Energy*, vol. 6, no. 1, pp. 55–70, 2020.

[32] E. J. Ransley, "Survivability of wave energy converter and mooring coupled system using CFD," 2015.

[33] L. Davidson, "An introduction to turbulence models," 2015.